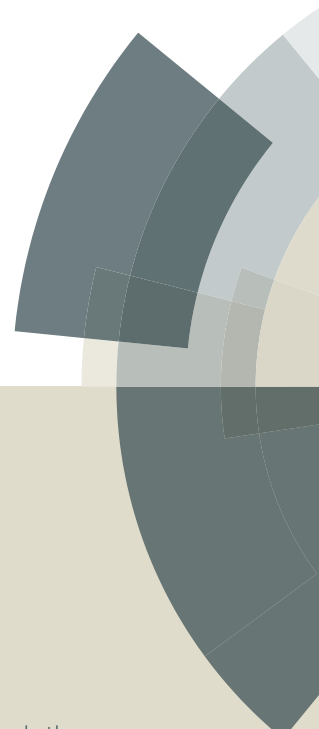


# JAAS

Accepted Manuscript



This article can be cited before page numbers have been issued, to do this please use: M. Bonta, J. Gonzalez, C. D. Quarles Jr., R. E. Russo, B. Hegedus and A. Limbeck, *J. Anal. At. Spectrom.*, 2015, DOI: 10.1039/C5JA00287G.



This is an *Accepted Manuscript*, which has been through the Royal Society of Chemistry peer review process and has been accepted for publication.

*Accepted Manuscripts* are published online shortly after acceptance, before technical editing, formatting and proof reading. Using this free service, authors can make their results available to the community, in citable form, before we publish the edited article. We will replace this *Accepted Manuscript* with the edited and formatted *Advance Article* as soon as it is available.

You can find more information about *Accepted Manuscripts* in the [Information for Authors](#).

Please note that technical editing may introduce minor changes to the text and/or graphics, which may alter content. The journal's standard [Terms & Conditions](#) and the [Ethical guidelines](#) still apply. In no event shall the Royal Society of Chemistry be held responsible for any errors or omissions in this *Accepted Manuscript* or any consequences arising from the use of any information it contains.

# Elemental mapping of biological samples by the combined use of LIBS and LA-ICP-MS

Maximilian Bonta<sup>1</sup>, Jhanis J. Gonzalez<sup>2,3†</sup>, C. Derrick Quarles Jr.<sup>2</sup>, Richard E. Russo<sup>2,3</sup>, Balazs Hegedus<sup>4,5</sup>, and Andreas Limbeck<sup>1\*</sup>

<sup>1</sup>TU Wien, Institute of Chemical Technologies and Analytics, Vienna, Austria

<sup>2</sup>Applied Spectra, Inc., Fremont, CA

<sup>3</sup>Lawrence Berkeley National Laboratory, Environmental Energy Technologies Division, Berkeley, CA

<sup>4</sup>Department of Thoracic Surgery, Comprehensive Cancer Center, Medical University of Vienna

<sup>5</sup>MTA-SE Molecular Oncology Research Group, Hungarian Academy of Sciences, Budapest

\*Corresponding authors:

TU Wien, Institute of Chemical Technologies and Analytics, Getreidemarkt 9/164-IAC, 1060 Vienna, Austria; Email: andreas.limbeck@tuwien.ac.at

<sup>†</sup>Applied Spectra, Inc., Fremont, CA, USA. Email: Jhanis@appliedspectra.com

<sup>†</sup>Lawrence Berkeley National Laboratory, Environmental Energy Technologies Division, Berkeley, CA, USA. Email: jjgonzalez@lbl.gov

## Abstract

In this study a combination of Laser Ablation Inductively Coupled Plasma Mass Spectrometry (LA-ICP-MS) and Laser Induced Breakdown Spectroscopy (LIBS) were used for laterally resolved elemental analysis of biological samples. In general LA-ICP-MS is an excellent technique for the analysis of many trace elements. However, bulk components such as H or O are not accessible using this technique. In addition to those elements, also some other elements that are difficult or impossible to investigate using LA-ICP-MS (i.e., F, N, Cl, etc.), could be detected by LIBS. In this work, the simultaneous use of LIBS and LA-ICP-MS (Tandem LA/LIBS) for the analysis of biological samples is presented, opening the door for the possibility of complete analysis of the elemental composition of a human tumor sample. Results show good correlation with the histological stainings. The obtained distribution images provide a valuable basis for further medical interpretation.

## Introduction

In various fields of research, Laser Ablation-Inductively Coupled Plasma-Mass Spectrometry (LA-ICP-MS) is accepted as a powerful tool for laterally resolved analysis of trace elements [1-3]. Life sciences are one of the most prominent fields of LA-ICP-MS imaging, besides geology and geochemistry [4, 5]. A great feature for this type of analysis is that thin-cut tissue samples can be analyzed just like they are commonly used in medical research (e.g., histological studies). Comparison between trace element distributions with histological stainings of consecutive tissue slices can help to investigate biological processes in closer detail than it is possible with

conventional methods used in clinical research. Over the last few years, numerous applications on various tissue types (e.g., kidney [6], brain [7], tumor tissues [8, 9]) have been presented. Even if LA-ICP-MS can complement the information obtained from histological investigations, one important aspect is not covered: more than 95% of the mass of a typical biological tissue are comprised of the elements C, H, N, O, P, and S, which are the main building blocks of organic matter. However, as LA-ICP-MS is not capable of analyzing H, N, and O, a full elemental analysis of a tissue specimen is not possible. Furthermore, the analysis of C using LA-ICP-MS is prone to a variety of problems, such as high background signal, unfavorable transport properties (i.e., partial transport in the form of gaseous carbon compounds), as well as a high first ionization potential compared to other common analytes [10].

Laser Induced Breakdown Spectroscopy (LIBS), is a powerful tool with access to every element in the periodic table with sensitivity in the medium  $\mu\text{g g}^{-1}$  range for most elements [11, 12]. Applications for the analysis of minor and trace elements in biological tissues have already been presented in the past [13, 14]. However, the concentration levels of the elements of interest in tissue samples are usually near or even below the detection limit of LIBS and thus, especially elemental mapping is often a difficult task [15]. Therefore, in order to obtain trace elemental composition from tissue samples at the same time as the major elements, LIBS data can be acquired simultaneously with LA-ICP-MS data. Thus, the analysis of one single sample, simultaneously using both techniques becomes feasible [16-18]. Therefore, LA-ICP-MS is used to analyze trace element components, whereas LIBS is used for the analysis of minor and major sample components including H and O. Besides expanding the elemental coverage range with the simultaneous use of LIBS and LA-ICP-MS, it also offers a few other advantages, such as simultaneous measurement of the complete spectral range and a very high sensitivity for alkaline and earth alkaline elements using LIBS. This can help to reduce the number of elements measured using LA-ICP-MS, which, in the case of typically used quadrupole or sectorfield mass analyzers, could lead to more precise results, especially important for isotope ratio investigations and quantitative analyses. Another beneficial aspect of this approach is that elements with  $m/z$  ratios being biased by spectral interferences (e.g., Mg, polyatomic interference by C-C, or C-N species on all isotopes) can be detected using LIBS without those interferences.

In this work, an instrument capable of simultaneously performing LIBS and LA-ICP-MS measurements (Tandem LA/LIBS) was used to develop a procedure for the analysis of biological samples with an expanded elemental coverage. Measurement parameters for both the LIBS and LA-ICP-MS were systematically optimized. Subsequently, this method was applied to a human tumor slice from an individual previously treated with cisplatin as anti-cancer drug. The simultaneous analysis of platinum (typically around  $10 \mu\text{g g}^{-1}$  in the tissue), naturally occurring trace elements in the tissue (Fe, Ni, ...), as well as major elements (C, H, O) has been performed, leading to an increased value for this type of elemental analysis. The use of Tandem LA/LIBS for the elemental mapping of biological tissues will also give rise to improved quantification approaches and new ways for tissue analysis.

## Experimental

### Chemicals

Ultra-pure water (resistivity  $18.2 \text{ M}\Omega \text{ cm}$ ) dispensed from a Barnstead EASYPURE II water system (ThermoFisher Scientific, Marietta, OH) was used for all experiments. (3-aminopropyl)-triethoxysilane (APES), as well as acetone were of analytical grade and were purchased from Sigma-Aldrich, Buchs, Switzerland.

## Instrumentation

All experiments were performed using a J200 Tandem LA/LIBS instrumentation (Applied Spectra Inc., Fremont, CA) equipped with a 266 nm frequency quadrupled Nd:YAG laser. For collection and spectroscopic analysis of the radiation emitted by the laser induced plasma, an optical fiber system connected to a Czerny-Turner spectrometer with a six-channel CCD detection was employed. For every laser shot, full spectra over the wavelength range from 190 to 1040 nm were recorded in Axiom data acquisition software provided by the manufacturer of the instrument. ICP-MS analysis of the generated aerosol was performed using a Thermo iCAP Qc quadrupole ICP-MS device (ThermoFisher Scientific, Bremen, Germany) and Qtegra data acquisition software (ThermoFisher Scientific, v.2.4). Connection of the Tandem LA/LIBS system to the mass spectrometer was achieved using PTFE tubing. Helium at a flow rate of 0.8 L min<sup>-1</sup> was used as ablation gas; argon at a flow rate of 0.8 L min<sup>-1</sup> was admixed to the He gas stream directly after the ablation chamber outlet to be used as make-up gas. LIBS and LA-ICP-MS analysis were run from the same sample spots simultaneously.

The instrumental performance of the LIBS system, as well as the LA-ICP-MS device were checked on a daily basis using NIST612 glass standard (trace elements in glass, National Institute of Standards and Technology, Gaithersburg, MD) to ensure constant operating conditions of the used instrumentation. For LIBS, the intensity of multiple wavelengths distributed over a wide wavelength range (Mg(I) 285.213 nm, Ca(II) 315.887 nm, Ba(II) 455.403 nm, Li(I) 670.776 nm, Rb(I) 780.027 nm) was investigated. The ICP-MS settings were optimized for maximum sensitivity for the <sup>115</sup>In signal. The oxide rate (measured by the <sup>140</sup>Ce<sup>16</sup>O/<sup>140</sup>Ce ratio) was kept below 1.9%; doubly charged ions (determined by Ba<sup>++</sup>/Ba<sup>+</sup>) were below 3%. Typical instrumental parameters of the measurements are summarized in Table 1.

Table 1: Optimized measurement parameters used for the presented experiments

<b>laser ablation system</b>	
laser output energy [mJ]	21.5
laser ablation crater [μm]	40
laser repetition rate [Hz]	2
stage scan speed [μm s <sup>-1</sup> ]	80
carrier gas flow (He) [L min <sup>-1</sup> ]	0.8
make-up gas flow (Ar) [L min <sup>-1</sup> ]	0.8
<b>spectrometer system (Czerny-Turner)</b>	
detection channels	6
Detector	CCD
gate delay [μs]	0,1
gate width [ms]	1.05
<b>ICP-MS (Thermo iCAP Q)</b>	
coolant gas flow (Ar) [L min <sup>-1</sup> ]	15.0
auxiliary gas flow (Ar) [L min <sup>-1</sup> ]	0.8
RF power [W]	1550
dwel time per isotope [ms]	10
cones	Ni
measured isotopes	<sup>31</sup> P, <sup>56</sup> Fe, <sup>57</sup> Fe, <sup>63</sup> Cu, <sup>65</sup> Cu, <sup>64</sup> Zn, <sup>68</sup> Zn, <sup>194</sup> Pt, <sup>195</sup> Pt, <sup>197</sup> Au

Visual images of the samples were taken using an optical microscope in reflective-light mode (Leica DM2500M, Leica Microsystems, Wetzlar, Germany).

### Preparation of printed patterns

For optimization of the measurement parameters, printed patterns on paper were used. They were prepared as described earlier by Bonta *et al.* [19]. Blue printer ink from a conventional office color laser printer was deposited in defined structures onto conventional white paper. Single patterns were cut out and attached to microscopic glass slides using double sided tape. Copper (contained in pigment of blue ink) was the analyte of interest for the optimization experiments of the LA-ICP-MS parameters.

### Preparation of tissue cryo-cuts and sample pretreatment

Silicon wafers (Infineon, Villach, Austria) were found to provide optimal properties as carrier material for elemental analysis of tissue cryo-cuts. Especially the low background signal for all elements of interest, compared to glass slides, was a favorable aspect. However, preliminary experiments showed that tissue thin-cuts would not tightly attach to the silicon wafer. Therefore, surface modification of the wafers was performed. According to a protocol published by Maddox and Jenkins [20], the natural SiO<sub>2</sub>-surface of the wafers was silylated using (3-aminopropyl)-triethoxysilane APES. This procedure forms a thin layer of basic moieties on the silicon wafers, providing optimal linkage with the acidic amino acid groups of the proteins in the tissue. 500 µL of APES (stored under inert gas) were mixed with 10 µL high purity water and 25 mL acetone. The clean and dry silicon wafers were immersed in the mixture for one minute. Subsequently, the treated wafers were transferred into a bath of high purity water, where they were kept for 2 minutes. Subsequently, the wafers were removed from the water bath and allowed to dry under ambient conditions.

Snap frozen surgical tissue specimen were attached to a sample holder using Shandon Cryomatrix (Thermo Scientific, Cat. no. 6769006). 20 µm thick sections were cut using a cryotome (Leica CM3050 S) at -20°C. The produced thin sections of the tissues were deposited onto the surface-modified silicon wafers and air-dried at room temperature. After deposition on the silicon wafers, the tissue thin sections were coated with a thin gold layer used as a pseudo-internal standard for LA-ICP-MS analysis. Coating was performed using an Agar B7340 sputter coater (Agar Scientific Ltd., Essex, UK) equipped with a target from high purity gold. Sputter conditions were set as reported previously [21].

### Simultaneous LIBS and LA-ICP-MS measurements and image construction

The sample surfaces (i.e., printed patterns and tissue sections) were scanned by the laser beam using a linescan pattern. All lines were scanned in the same direction, with a break of five seconds between the ablation of two lines. The horizontal distance between single lines was chosen to be the size of the ablation crater. In preliminary experiments, the optimal laser settings were evaluated. It was desired that the complete sample material on one location was ablated with one laser shot. Additionally, the stage scanning speed had to be adjusted in order to provide short measurement times without considerable washout effects on the LA-ICP-MS signal. Evaluation of the scan speed was performed using the metric area mismatch percentage (AMP) introduced by Bonta *et al.* [19]. Microscopic images of the patterns were compared with the elemental distributions obtained from the LA-ICP-MS measurements. The AMP value was calculated, describing the differences between the two images, and thus, the image quality of the elemental distribution image.

LIBS distribution images were constructed using the knowledge about the exact position of one ablation location. Peaks were chosen manually, background correction was performed for every peak by subtracting the integral of a nearby area, which exhibited only background signal. Time-resolved intensity data obtained from the LA-ICP-MS measurements were converted into distribution images using a data import routine in ImageLab (v.1.00, Epina GmbH., Pressbaum, Austria) [22]. The data acquired by both domains were combined in ImageLab, which allows the processing of multisensor imaging data.

## Results

### Optimization of the measurement parameters for simultaneous LIBS and LA-ICP-MS analysis

In order to optimize the measurement process for both parts of the analysis, several parameters had to be taken into consideration. All measurement parameters were optimized considering the fact that the final distribution image should have a lateral resolution of 40  $\mu\text{m}$  per pixel. This resolution was found to be sufficient for medical interpretation of the results, while keeping the measurement time as low as possible.

#### *Optimization of the LIBS parameters for measurement of biological samples*

The LIBS signal for the analyzed bulk components of the tissue (C, H, and O) should be optimized in order to obtain highest signal intensities for these elements. A tissue thin cut was used for optimization of the LIBS parameters. Compared to typical solid samples, in the case of tissue thin-cuts, the whole sample material is ablated. To ensure complete ablation of the sample material across the whole area covered by the laser beam (i.e., to obtain the maximum LIBS signal per sample location), the laser output energy was chosen to fully ablate the sample material in one shot. Furthermore, stage scan speed and repetition rate were set in a way that consecutive laser shots would not overlap. Thus, at a laser beam diameter of 40  $\mu\text{m}$  (equal to the area of material ablation), for example, a laser repetition rate of 1 Hz and a stage scan speed of 40  $\mu\text{m s}^{-1}$  would be feasible. Also other pairs of settings were possible, however, if the ratio of repetition rate and stage scan speed was constant, the LIBS signal should not be influenced. The dependence of stage scan speed and image quality should be investigated in a later step.

If laser spot size and the ratio of repetition rate and stage scan speed were constant, the remaining parameters influencing the detected signal intensity were laser energy and gate delay of the spectrometer. A full factorial design of experiments (DoE) was carried out, to define the optimal settings. Thus, a set of feasible parameters was chosen to be examined. Laser output energies providing complete yet controlled ablation of the sample material using a single shot (23.0, 21.5, 16.6, and 12.3 mJ), as well as spectrometer gate delays of 0.05, 0.1, 0.2, and 0.5  $\mu\text{s}$  were taken into consideration for the optimization. In preliminary measurements of human tissue samples, the carbon emission line at 247.856 nm showed to have the weakest abundance, compared to hydrogen at 656.279 nm and oxygen at 777.421 nm. While the other analytes were still monitored, DoE was carried out for the emission line of carbon. Relative standard deviations of the yielded intensities were always below 10% (n=10).

The background corrected signals of the carbon emission line at 247.856 nm showed the highest intensity at a laser output energy of 21.5 mJ and a spectrometer gate delay of 0.1  $\mu\text{s}$ . Thus, these parameters were selected for the following experiments. The chosen settings also allow satisfactory detection of hydrogen and oxygen. The general trend of the results shows that

shorter spectrometer gate delays and higher laser output energies promote the intensity of the carbon signal.

#### *Optimization of the LA-ICP-MS parameters*

Compared to LIBS, where the emission spectrum of every laser pulse is collected, for LA-ICP-MS, the washout time of the ablation cell is a crucial parameter. The range of feasible measurement settings is already very limited by the favorable factors for the LIBS part of the experiment. Thus, only four pairs of laser repetition rate and stage scan speed (with a constant ratio of these two values) were evaluated. All other parameters were kept constant, as they had already been optimized for the LIBS measurements. Printed patterns on paper containing copper as the analyte of interest were used for this optimization step. Definition of the most favorable parameters for LA-ICP-MS measurement was performed according to a procedure proposed by Bonta *et al.* [19]. Printed patterns on paper were used to determine the laser settings which would depict the actual distribution of the analyte in the best way. A visual image of the printed sample was compared with the measured elemental distribution image at each laser setting. The metric 'area mismatch percentage' (AMP) was employed for this task. While the laser output energy was kept at 21.5 mJ and the ablation crater diameter at 40  $\mu\text{m}$ , stage scan speed and laser repetition rate were altered (1 Hz/0.04  $\text{mm s}^{-1}$ , 2 Hz/0.08  $\text{mm s}^{-1}$ , 5 Hz/0.20  $\text{mm s}^{-1}$ , 10 Hz/0.40  $\text{mm s}^{-1}$ ). The determination of the AMP value was carried out in three replicate measurements.

A laser repetition rate of 2 Hz at a stage scan speed of 80  $\mu\text{m s}^{-1}$  exhibits the lowest AMP value, i.e., the best conditions for optimal representation of the actual elemental distribution in the LA-ICP-MS image. The appearing trend of the AMP values can be explained easily: Slower scan speeds lead to an inconstant signal course, as most of the sample aerosol will already be washed out prior to the next laser pulse. Faster scan speeds will create image blurring owing to incomplete washout of the ablation cell when already ablating the next location.

#### **Analysis of a tissue sample using the optimized conditions**

By a combination of the two performed optimization steps, the best measurement settings for a simultaneous LIBS and LA-ICP-MS measurement could be determined. The optimized dependent variables were signal intensity (for LIBS) and image accuracy (for LA-ICP-MS).

To obtain a general overview about the elements to be analyzed by the LIBS-domain of the system, a scan across 1  $\text{mm}^2$  of a representative area of a tumor sample was performed. Measurements were performed as linescans; the optimized parameters were used for the measurements. An area without sample material was ablated using the same instrumental settings, to obtain a blank spectrum of the sample carrier material (silicon wafer). A blank-subtracted LIBS spectrum of the investigated sample area is presented in Figure . 100 spectra acquired from single laser shots were accumulated for this spectrum.

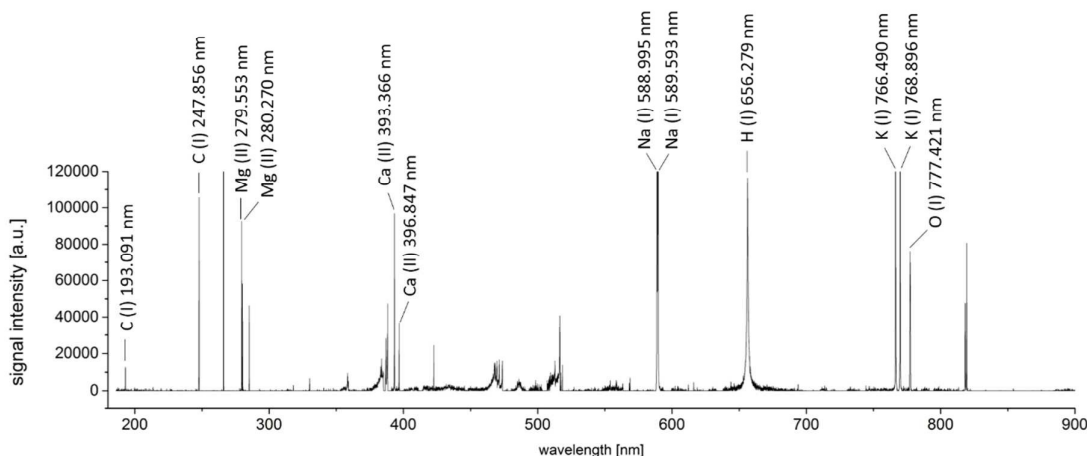


Figure 1: LIBS spectrum of a tissue sample, accumulated signals from 100 laser shots

Besides the element of interest, also alkaline (Na, K) and earth alkaline elements (Ca, Mg) can be identified. Typically, abundances of these elements in biomaterials are rather high [23] and LIBS measurements are very sensitive for those elements. Thus, monitoring of these sample constituents using LA-ICP-MS was omitted, as analysis using LIBS showed to be feasible. Abundances of typical trace elements in biological tissues, as well as the administered drug were considered for selection of the isotopes for LA-ICP-MS measurement, yielding count rates ranging some thousand counts per second ( $^{195}\text{Pt}$ ) to several hundred thousand counts for  $^{56}\text{Fe}$ .

### Elemental mapping of a human tumor sample

Elemental mapping of tumor sections for their metal content using LA-ICP-MS, is already well established in the life sciences. However, also information about the bulk elements of biological tissues might be of important value to give information about tissue composition, which can be obtained using LIBS. Thus, in this study, simultaneous mapping of trace and bulk elements using a simultaneous LIBS and LA-ICP-MS system was performed. The measurement parameters determined during the optimization procedure described above were used for the elemental mapping experiment. A cryo-cut of a human malignant pleural mesothelioma (MPM) sample with a thickness of 20  $\mu\text{m}$  deposited on a surface-modified silicon wafer was fully ablated during one cycle of analysis. To correct instrumental drifts of the ICP-MS device during operation, the  $^{197}\text{Au}$  signal, derived from a sputtered gold layer on the sample surface, was used as a pseudo-internal standard. The elemental distribution images for selected elements (lateral resolution 40  $\mu\text{m}$ ) are displayed in Figure .

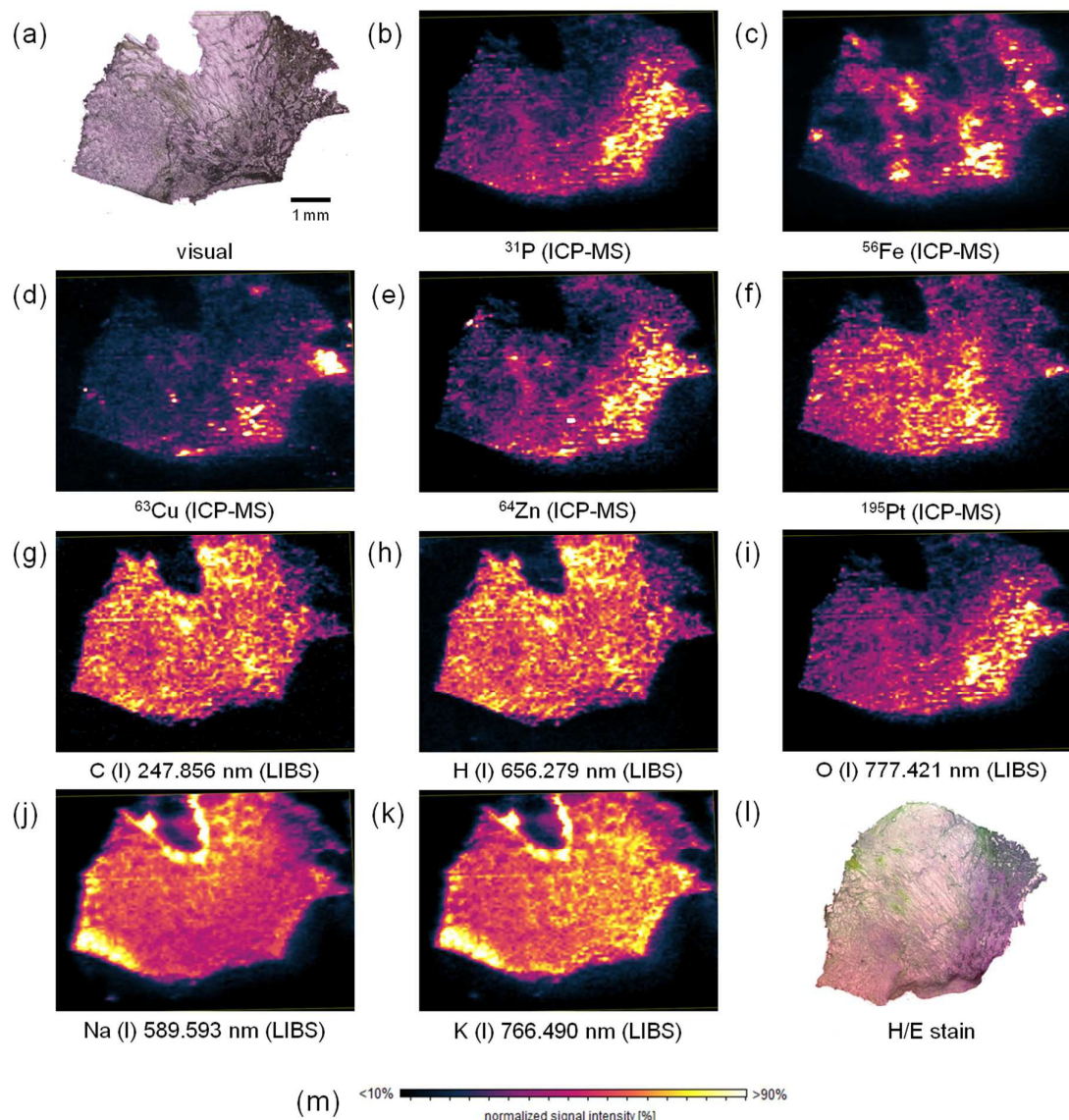


Figure 2: Microscopic image of the analyzed sample (a), elemental images of  $^{31}\text{P}$  (b),  $^{56}\text{Fe}$  (c),  $^{63}\text{Cu}$  (d),  $^{64}\text{Zn}$  (e), and  $^{195}\text{Pt}$  (f) determined by LA-ICP-MS, elemental distributions of carbon (g), hydrogen (h), oxygen (i), sodium (j), and potassium (k) measured using LIBS, a consecutive tissue thin-cut after hematoxylin and eosin staining (l), color scale for the displayed images (m)

The hematoxylin and eosin staining of a consecutive tissue thin-cut displayed in Figure l reveals areas with tumor tissue (purple) and regions without viable tumor cells (pink). The two consecutive tissue slices are not perfectly matching. Still, areas with viable tumor cells can be identified. Together with this information, the obtained elemental distributions can be interpreted. The bulk elements carbon and hydrogen (Figure g and 2h) are rather homogeneously distributed over the thin section of the tissue. Still, some areas show altered signal intensities, most probably indicating higher or lower tissue density in the respective regions. Also differing tissue thickness might be contributing to these signal changes. The distributions of carbon and hydrogen show a numerical correlation. Linear regression of the

1  
2  
3  
4  
5  
6  
7  
8  
9  
10  
11  
12  
13  
14  
15  
16  
17  
18  
19  
20  
21  
22  
23  
24  
25  
26  
27  
28  
29  
30  
31  
32  
33  
34  
35  
36  
37  
38  
39  
40  
41  
42  
43  
44  
45  
46  
47  
48  
49  
50  
51  
52  
53  
54  
55  
56  
57  
58  
59  
60

signal intensities of corresponding pixels yielded a correlation coefficient of 0.9599. This finding leads to the conclusion that the C/H-ratio is rather constant throughout the tissue. In comparison, phosphorus (Figure b) and oxygen (Figure i) exhibit heterogeneous distribution throughout the section. Higher intensities of these two elements correlate well with the tumor regions (especially in the right part of the tissue). A good correlation between the distributions of the elements might point towards a high phosphate concentration in those regions. This could be explained by a high number of activated proteins (i.e., phosphorylated species), high DNA content, and a high amount of phospholipids in the tumor regions. All these compounds can be found in a higher concentration in tumor tissue, as the growth rate of the cells is increased in such tissue areas. Zinc (Figure e) and copper (Figure d) exhibit similar distributions. These elements are important trace elements and often acting as cofactors of proteins. Notable examples of proteins employing Cu and/or Zn as cofactors are for example superoxide dismutase (SOD) [24], or some ATPases [25]. These proteins are essential for tackling oxidative intracellular stress (SOD), and for protein phosphorylation (ATPases).

Compared to analytes detected with higher signal intensities in the tumor tissue, platinum (Figure f), originating from the treatment of the patient with cisplatin, a commonly used anti-cancer drug, is rather accumulated in healthy tissue areas. This effect has already been described earlier [8]. Probably, the drug has not yet entered these regions, or some resistance mechanisms occur, which hamper drug uptake.

Iron (Figure c) exhibits a very inhomogeneous distribution across the tissue sample. However, no histologically relevant structures can be correlated with the obtained elemental distribution. As with copper and zinc described before, also iron is an important cofactor for many proteins [26] with functions for example in oxygen transport or energy storage. Sodium (Figure j) and potassium (Figure k) are homogeneously distributed. The distributions have a good numerical correlation ( $R^2=0.8781$ ), potassium shows slightly higher signal intensities in the tumor area. The v-shaped structure in the upper part of the image can be related to a contamination from the embedding medium. The increased intensities of both signals in the left part of the tissue sample cannot be explained. The biological function of sodium and potassium is closely related: A Na/K-gradient keeps up the membrane pressure of the cells and therefore helps to maintain their state [27]. Magnesium and calcium exhibit similar distributions (not shown). These two elements also have similar functions in organisms. Both play a pivotal role in signal transduction [28].

## Conclusion

In the presented study, the simultaneous use of LIBS and LA-ICP-MS (Tandem LA/LIBS) has been used for elemental mapping of trace and bulk elements in biological tissues. After thorough method optimization, a human tumor sample has been investigated to show the applicability of this technique. The benefits of of this simultaneous application using LA-ICP-MS and LIBS for the analysis of biological samples were highlighted: while LA-ICP-MS is perfectly suited for the laterally resolved analysis of trace elements in the tissue (e.g., Fe, Zn, Cu), LIBS is optimal for mapping of major (C, H, O) and minor elements (Na, K, Ca, Mg) in biological tissues. LIBS also allows the analysis of elements that are affected by high background signals (e.g., K), or polyatomic interferences (e.g., Mg) when employing ICP-MS detection. Most common mass analyzers used for ICP-MS devices operate on a sequential basis (today, only a small fraction of instruments employs time-of-flight or other simultaneous mass analyzers), reducing the number of isotopes monitored by LA-ICP-MS will also increase the accuracy of measurement for the remaining analytes. Thus, the parallel use of LIBS complements classical LA-ICP-MS in many aspects and its application for elemental mapping of biological samples represents a number of improvements. Biological functions of the trace elements could be well correlated with their

1  
2  
3  
4  
5  
6  
7  
8  
9  
10  
11  
12  
13  
14  
15  
16  
17  
18  
19  
20  
21  
22  
23  
24  
25  
26  
27  
28  
29  
30  
31  
32  
33  
34  
35  
36  
37  
38  
39  
40  
41  
42  
43  
44  
45  
46  
47  
48  
49  
50  
51  
52  
53  
54  
55  
56  
57  
58  
59  
60

respective distributions. The additional information obtained by using LA-ICP-MS and LIBS simultaneously might yield information which is also relevant for medical questions. For example, the well correlated phosphorus and oxygen distributions suggest a high abundance of phosphates. Such information can help to make the results of elemental analysis more valuable for the use in drug development and medication.

## Acknowledgment

The research was supported by the Office of Basic Energy Sciences, Chemical Science Division and the Defense Nuclear Nonproliferation Research and Development Office of the U.S. Department of Energy under contract number DE-AC02-05CH11231 at the Lawrence Berkeley National Laboratory. M.B. wants to acknowledge the MEIBio PhD program of the TU Wien for providing a scholarship for the period 2013–2016.

## References

1. Mokgalaka, N.S. and J.L. Gardea-Torresdey, *Laser Ablation Inductively Coupled Plasma Mass Spectrometry: Principles and Applications*. Applied Spectroscopy Reviews, 2006. **41**(2): p. 131-150.
2. Günther, D. and B. Hattendorf, *Solid sample analysis using laser ablation inductively coupled plasma mass spectrometry*. TrAC Trends in Analytical Chemistry, 2005. **24**(3): p. 255-265.
3. Russo, R.E., et al., *Laser Ablation in Analytical Chemistry*. Analytical Chemistry, 2013. **85**(13): p. 6162-6177.
4. Becker, J.S., et al., *Bioimaging of metals by laser ablation inductively coupled plasma mass spectrometry (LA-ICP-MS)*. Mass Spectrom Rev, 2010. **29**(1): p. 156-75.
5. Hare, D., C. Austin, and P. Doble, *Quantification strategies for elemental imaging of biological samples using laser ablation-inductively coupled plasma-mass spectrometry*. Analyst, 2012. **137**(7): p. 1527-1537.
6. Moreno-Gordaliza, E., et al., *Elemental bioimaging in kidney by LA-ICP-MS as a tool to study nephrotoxicity and renal protective strategies in cisplatin therapies*. Anal Chem, 2011. **83**(20): p. 7933-40.
7. Becker, J.S., et al., *Bioimaging of metals in brain tissue by laser ablation inductively coupled plasma mass spectrometry (LA-ICP-MS) and metallomics*. Metallomics, 2010. **2**(2): p. 104-11.
8. Bonta, M., et al., *Quantitative LA-ICP-MS imaging of platinum in chemotherapy treated human malignant pleural mesothelioma samples using printed patterns as standard*. Journal of Analytical Atomic Spectrometry, 2014. **29**(11): p. 2159-2167.
9. Hare, D., et al., *Elemental bio-imaging of melanoma in lymph node biopsies*. Analyst, 2009. **134**(3): p. 450-3.
10. Frick, D.A. and D. Günther, *Fundamental studies on the ablation behaviour of carbon in LA-ICP-MS with respect to the suitability as internal standard*. Journal of Analytical Atomic Spectrometry, 2012. **27**(8): p. 1294-1303.
11. Hahn, D.W. and N. Omenetto, *Laser-induced breakdown spectroscopy (LIBS), part II: Review of instrumental and methodological approaches to material analysis and applications to different fields*. Applied Spectroscopy, 2012. **66**(4): p. 347-419.

12. Miziolek, A.W., V. Palleschi, and I. Schechter, *Laser induced breakdown spectroscopy (LIBS): Fundamentals and applications*. Laser Induced Breakdown Spectroscopy (LIBS): Fundamentals and Applications. 2006. 1-620.
13. Kaiser, J., et al., *Trace elemental analysis by laser-induced breakdown spectroscopy - Biological applications*. Surface Science Reports, 2012. **67**(11-12): p. 233-243.
14. Santos Jr, D., et al., *Laser-induced breakdown spectroscopy for analysis of plant materials: A review*. Spectrochimica Acta - Part B Atomic Spectroscopy, 2012. **71-72**: p. 3-13.
15. Sancey, L., et al., *Laser spectrometry for multi-elemental imaging of biological tissues*. Scientific Reports, 2014. **4**.
16. Dong, M., et al., *Elemental analysis of coal by tandem laser induced breakdown spectroscopy and laser ablation inductively coupled plasma time of flight mass spectrometry*. Spectrochimica Acta - Part B Atomic Spectroscopy, 2015. **109**: p. 44-50.
17. Subedi, K., T. Trejos, and J. Almíral, *Forensic analysis of printing inks using tandem laser induced breakdown spectroscopy and laser ablation inductively coupled plasma mass spectrometry*. Spectrochimica Acta - Part B Atomic Spectroscopy, 2015. **103-104**: p. 76-83.
18. Chirinos, J.R., et al., *Simultaneous 3-dimensional elemental imaging with LIBS and LA-ICP-MS*. Journal of Analytical Atomic Spectrometry, 2014. **29**(7): p. 1292-1298.
19. Bonta, M., et al., *A metric for evaluation of the image quality of chemical maps derived from LA-ICP-MS experiments*. Journal of Analytical Atomic Spectrometry, 2015.
20. Maddox, P.H. and D. Jenkins, *3-Aminopropyltriethoxysilane (APES): a new advance in section adhesion*. Journal of Clinical Pathology, 1987. **40**(10): p. 1256-1257.
21. Bonta, M., et al., *Application of gold thin-films for internal standardization in LA-ICP-MS imaging experiments*. Analyst, 2014. **139**(6): p. 1521-31.
22. <http://www.imagelab.at/>.
23. Carvalho, M.L., et al., *Trace elements in human cancerous and healthy tissues: A comparative study by EDXRF, TXRF, synchrotron radiation and PIXE*. Spectrochimica Acta Part B: Atomic Spectroscopy, 2007. **62**(9): p. 1004-1011.
24. Sarkar, B., *Metal protein interactions*. Prog Food Nutr Sci, 1987. **11**(3-4): p. 363-400.
25. Sitsel, O., et al., *Structure and function of Cu(I)- and Zn(II)-ATPases*. Biochemistry, 2015.
26. Lill, R., *Function and biogenesis of iron-sulphur proteins*. Nature, 2009. **460**(7257): p. 831-8.
27. Conway, E.J., *Principles underlying the exchanges of K and Na ions across cell membranes*. J Gen Physiol, 1960. **43**: p. 17-41.
28. Somjen, G.G. and G. Kato, *Effects of magnesium and calcium on neurones in the central nervous system*. Brain Res, 1968. **9**(1): p. 161-4.